Filamentation of interacting femtosecond laser pulses in air

Y.-Y. Ma · X. Lu · T.-T. Xi · Q.-H. Gong · J. Zhang

Abstract The filamentation of two co-propagated femtosecond (fs) laser pulses in air is studied by numerical simulation. Depending on the different initial separation distances, relative phase shift and crossing angles, simulations show attraction, fusion, repulsion and collision of the two pulses. A long plasma channel can be formed by two in-phase pulses with small separation distance and cross angle. The coupling of two laser beam becomes weaker when the separation distance or cross angle between two beams is larger. In this case, the filamentation of each pulse develops independently. Our simulation results will be helpful for understanding the effect of the initial amplitude and phase modulation of laser pulse on the filamentation characteristics.

PACS 52.38.Hb · 52.35.Mw

1 Introduction

The propagation of an ultrashort intense laser beam in the atmosphere has been the subject of interest during the last years due to its potential applications such as atmospheric remote sensing and lighting control [1–9]. If the peak power of the laser beam is many times higher than the self-focusing threshold $P_{cr} = \lambda^2/2\pi n_0 n_2$, the laser beam will break up into several filaments in space and several sub-pulses in time.

Recent experiments and numerical simulations show that the multi-filamentation phenomena may originate from the initial fluctuations of the intensity distribution of natural intense fs laser pulses [10–14]. In numerical studies, the envelope of the laser beam with initial fluctuation is usually taken as superposition of several Gaussian functions. S.A. Hosseini et al. numerically simulated the filamentation of intensity-modulated laser beams and revealed that the filamentation process strongly depends on the initial perturbations of the laser pulse [11]. O.G. Kosareva et al. performed simulations of a set of random initial pulse distribution propagating in air and revealed the effect of relative position between the perturbations on the plasma channel [14]. Earlier experiments showed that the phase distribution of fs laser pulse also has an effect on the filamentation characteristics [15, 16]. The interaction of in-phase and anti-phase beams in Kerr nonlinear media with different initial separation distances was studied analytically and numerically in Ref. [17], but the filamentation process after self-focusing was not considered. Ameil A. Ishaaya et al. [18] numerically and experimentally studied the self-focusing dynamics of coupled fs laser pulses in BK7 glass. The attraction and repulsion of the laser pulses were observed in the initial propagation stage, when multiphoton ionization is not significant.

The multi-filamentation process reshapes the laser pulses to a group of interacting filaments, and the plasma channel length under multi-filamentation is strongly dependent on the interaction characteristics of filaments. The interaction

Y.-Y. Ma · X. Lu · T.-T. Xi · J. Zhang (✉)
Laboratory of Optical Physics, Institute of Physics,
Chinese Academy of Sciences, Beijing 100190, China
e-mail: jzhang@aphy.iphy.ac.cn

Y.-Y. Ma · Q.-H. Gong · J. Zhang
State Key Laboratory for Mesoscopic Physics,
Department of Physics, Peking University, Beijing 100871, China

J. Zhang
Department of Physics, Shanghai Jiao Tong University,
Shanghai 200240, China

mechanism of filaments was numerically studied in our earlier work, where an envelope of a thin filament was taken as the initial laser field [9]. But actually the intensity and phase of a laser filament cannot be directly controlled. The multi-filamentation mode is usually regulated by changing the initial distribution of laser intensity and phase. In order to further understand the effect of initial distribution of the intensity and phase on the multi-filamentation characteristic in air, the systematic numerical simulations on the propagation of two identical Gaussian fs laser pulses with different separation distances, phase shifts and cross angles are presented in this paper. The attraction, fusion, repulsion, and collision of the two pulses are observed in the evolution of energy fluence and electron density in the simulations. The length of the plasma channel formed by two interacting laser beams strongly depends on the relative phase shift and the initial propagating direction of the pulses.

2 Numerical simulation model

The propagation of laser pulse in air is governed by an extended nonlinear Schrödinger equation together with the evolution equation for the electrons from multiphoton ionization [15]

$$\frac{\partial E}{\partial z} = \frac{i}{2k}\Delta_\perp E - i\frac{k''}{2}\frac{\partial^2 E}{\partial t^2} + ikn_2\Re(t)E$$
$$- ik\frac{\omega_{pe}^2(\rho)}{\omega_0^2}E - \frac{\beta^{(K)}}{2}|E|^{2K-2}E \tag{1a}$$

$$\Re(t) = (1-\vartheta)|E|^2 + \frac{\vartheta}{\tau_K}\int_{-\infty}^{t} e^{-(t-t')/\tau_K}|E(t')|^2 dt' \tag{1b}$$

$$\frac{\partial \rho}{\partial t} = \frac{\beta^{(K)}}{K\hbar\omega_0}|E|^{2K}\left(1 - \frac{\rho}{\rho_{at}}\right) \tag{2}$$

These equations are expressed in the reference frame moving with the pulse group velocity ($t \to t - z/v_g$), characterized by the central wave number $k = 2\pi/\lambda_0$, where $\lambda_0 = 800$ nm is the central wavelength of the laser beam in air. The terms on the right-hand side of (1a) account for the transverse diffraction with $\Delta_\perp \equiv \partial^2/\partial x^2 + \partial^2/\partial y^2$, the group velocity dispersion, the complete Kerr response of air, the defocusing induced by multiphoton ionization (MPI) and the power dissipation caused by multiphoton absorption (MPA) with coefficient $k'' = 0.2$ fs^2/cm, $n_2 = 3.2 \times 10^{-19}$ cm^2/W, $\beta^{(K=8)} = 4.25 \times 10^{-98}$ cm^{-13}/W^7 at 800 nm in air. The complete Kerr response of air, defined by (1b), is composed of an instantaneous contribution and a delayed part in ratio ϑ, with a relaxation time $\tau_K = 70$ fs [7]. The number of photons K needed to ionize electrons from molecular oxygen is $K = 8$. The plasma

frequency is $\omega_{pe} = \sqrt{q_e^2\rho/m_e\varepsilon_0}$ (q_e, m_e, and ρ are the electron charge, mass, and density, respectively), and the density of neutral atoms is $\rho_{at} = 2.7 \times 10^{19}$ cm^{-3}. We ignore the effect of self-steepening and space-time focusing. These effects mainly influence the temporal characteristics of the pulses which are not the main interest of our work.

3 Numerical simulations and discussions

We performed numerical simulations of the filamentation of single fs pulse for comparison. In our simulation, a laser beam with 40 fs duration is used to generate long range filament. The initial beam waist is 0.59 mm and the pulse energy is 1 mJ. The peak power of the pulse is five times larger than the self-focusing threshold P_{cr}. The laser beam has Gaussian shape in spatial and temporal domains

$$E(x, y, z, t)|_{z=0} = E_0 e^{(-(x^2+y^2)/r_0^2-t^2/\tau_0^2)} \tag{3}$$

Figure 1 shows the distributions of energy fluence (a) and electron density (b) for the laser pulse propagating in air. We can find that the filamentation of the laser beam starts at $z = 40$ cm and the filament can stably propagate over 0.5 m distance.

The initial electric-field of two co-propagated laser pulses is taken as the sum of two Gaussian functions

$$E(x, y, z, t)|_{z=0} = E_0\big(e^{-[(x-\Delta_0/2)^2+y^2]/r_0^2-t^2/\tau_0^2}$$
$$+ e^{i\varphi}e^{-[(x+\Delta_0/2)^2+y^2]/r_0^2-t^2/\tau_0^2}\big) \tag{4}$$

where Δ_0 and φ are the initial separation distance and relative phase shift between the two pulses, respectively. The parameters of each pulse are the same with the pulse in Fig. 1. Figure 2a illustrates the spatiotemporal intensity distribution of in-phase parallel Gaussian pulses with initial separation distances, $\Delta_0 = 0.78$ mm. It is shown that the two pulses collapse at $z = 30$ cm and temporally break
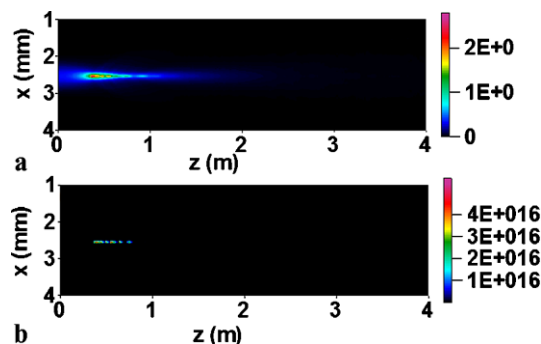

Fig. 1 **a** The energy fluence distribution (J/cm^2) and **b** electron density (/cm^3) of single beam's filamentation in air for the spatial slice at $y = 2.5$ mm

Fig. 2 **a** The spatiotemporal intensity distribution of two parallel in-phase interacting Gaussian pulses with the initial separation distance $\Delta_0 = 0.78$ mm. **b**, **c**, **d**, **e** The energy fluence distributions (J/cm^2) of two parallel in-phase interacting Gaussian pulses with different initial separation distance $\Delta_0 = 0.62$ mm (**b**), 0.78 mm (**c**), 0.94 mm (**d**), and 1.09 mm (**e**). All the figures are plotted for the spatial slice at $y = 2.5$ mm
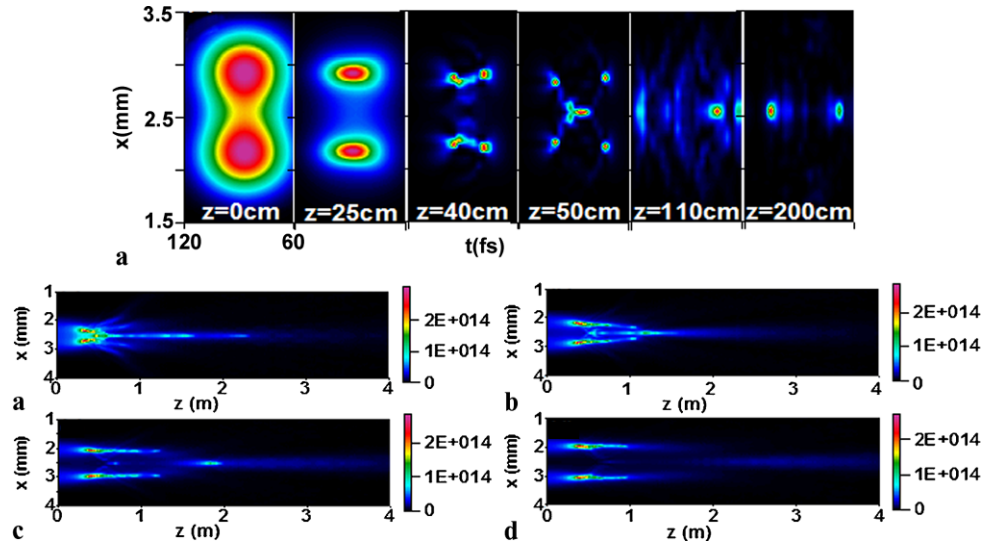
Fig. 3 The electron densities $(/cm^3)$ for two parallel in-phase interacting Gaussian pulses with the initial separation distance $\Delta_0 = 0.62$ mm (**a**), 0.78 mm (**b**), 0.94 mm (**c**), and 1.09 mm (**d**). All the figures are plotted for the spatial slice at $y = 2.5$ mm
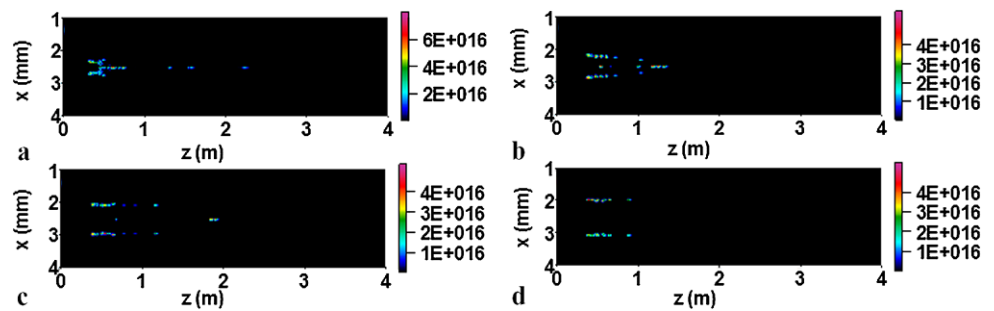

into two subpulses at $z = 50$ cm, respectively. The filaments then defocus by the induced plasma and more energy disperses outside. Because the two pulses interfere constructively, the intensity in the overlapping region becomes larger which leads to a larger refractive index in the center due to the Kerr effect. Thus the background energy is attracted towards the center, resulting in a new filament at $z = 110$ cm. Figure 2b, c, d, e show the interaction of two in-phase parallel Gaussian pulses with different initial separation distances, $\Delta_0 = 0.62$ mm (b), 0.78 mm (c), 0.94 mm (d) and 1.09 mm (e). The initial separation distance plays an important role in the interaction of the pulses. If the initial separation distance is comparable to the waist of each pulse (Fig. 2b), the merging process starts earlier. The merging of filaments prolongs the filament's length and the plasma channel's length (Fig. 3) by comparison with filamentation of a single beam. When the separation distance is much larger than the initial transverse waist of each Gaussian pulses, the filamentation of each pulse developed independently (Fig. 2e). We can find that the peaks of electron density generated in both merging (Fig. 3a, b, c) and non-merging (Fig. 3d) cases are at $10^{16}(/cm^3)$ level (Fig. 3).

When the two laser beams are out-of-phase, the destructive interference leads to reduction of the intensity of the

beam in the overlapping region. This results in the decrease of refractive index in the center and more laser energy disperses to outside. When the initial separation distance is less than the transverse waist of the initial Gaussian beam, due to the strong overlapping of laser field, the two out-of-phase pulses will directly repulse each other and disperse quickly. The collapsing to thin filaments was not observed, as shown in Fig. 4a and b. The electron densities generated are very low (Fig. 5a and b). For large separation distances, each beam produces one thin filament and the two filaments repel each other, as shown in Fig. 4c and d. The length of the plasma channel under this situation (Fig. 5c and d) is a bit smaller than that formed by a single pulse. Figure 6 illustrates the interaction of two parallel pulses with different phase shifts, $\varphi = 0.25\pi$ (a), 0.5π (b) and 0.75π (c). The separation distance is fixed on $\Delta_0 = 0.62$ mm. It is shown that phase shift between the two beam is also essential in the propagation. If the phase shift is $0 < \varphi < 0.5\pi$, the two collapsing pulses also attract and fuse (Fig. 6a and b) but the phase shift between the two pulses induces asymmetric distribution of the phase plane which causes the complex energy exchange between them. Then the two pulses merge together later on. The length of the plasma channel formed during this process becomes shorter (Fig. 7a). When the relative phase shift between two pulses exceeds 0.5π,

Fig. 4 The energy fluence distributions (J/cm^2) of two parallel out-of-phase interacting Gaussian pulses with different initial separation distance $\Delta_0 = 0.31$ mm (**a**), 0.47 mm (**b**), 0.94 mm (**c**), and 1.09 mm (**d**). All the figures are plotted for the spatial slice at $y = 2.5$ mm
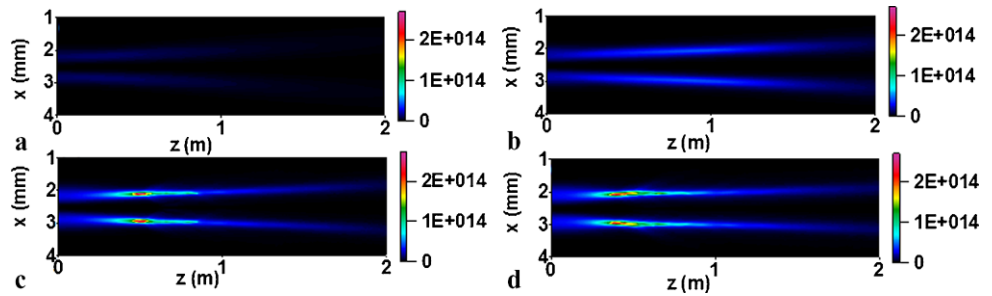
Fig. 5 The electron densities (/cm^3) for two parallel out-of-phase interacting Gaussian pulses with the initial separation distance $\Delta_0 = 0.31$ mm (**a**), 0.47 mm (**b**), 0.94 mm (**c**), and 1.09 mm (**d**). All the figures are plotted for the spatial slice at $y = 2.5$ mm
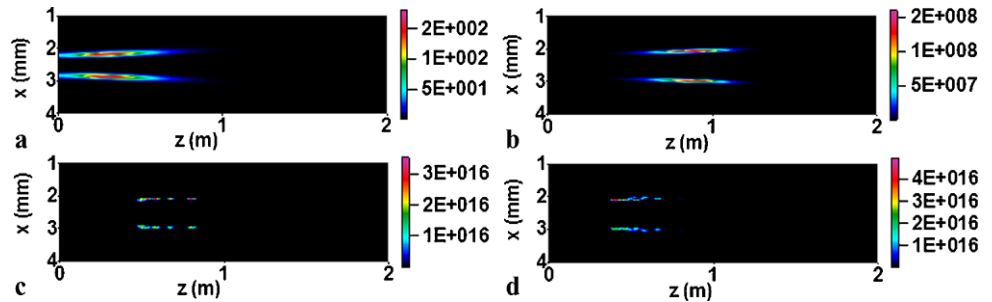
Fig. 6 The energy fluence distributions (J/cm^2) of two interacting parallel pulses with a fixed separation distance of $\Delta_0 = 0.62$ mm and different phase shift, $\varphi = 0.25\pi$ (**a**), 0.5π (**b**), and 0.75π (**c**). All the figures are plotted for the spatial slice at $y = 2.5$ mm
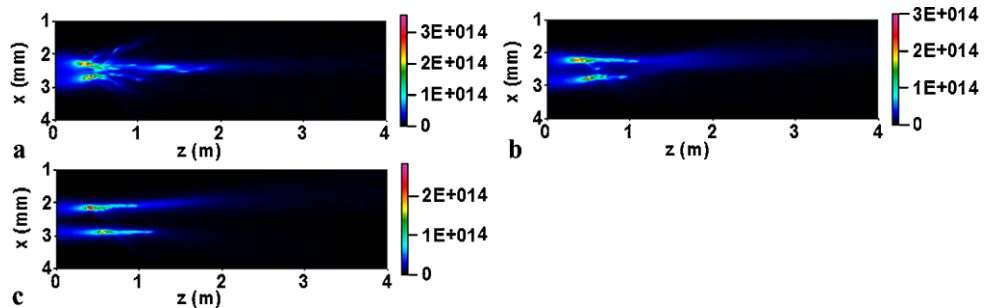
Fig. 7 The electron densities (/cm^3) for two parallel interacting Gaussian pulses with different phase shift, $\varphi = 0.25\pi$ (**a**), 0.5π (**b**), and 0.75π (**c**). The initial separation distance is $\Delta_0 = 0.62$ mm. All the figures are plotted for the spatial slice at $y = 2.5$ mm
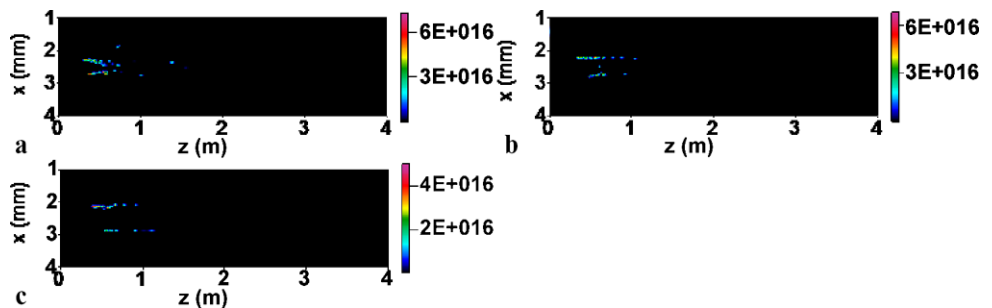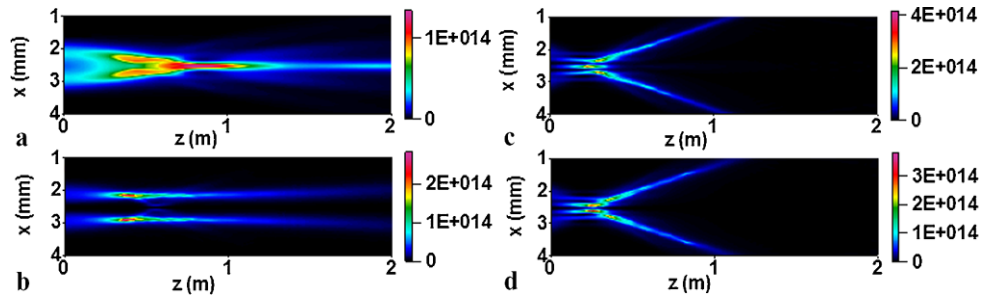
the two collapsing beams exhibit obvious repulsion process. As a result, in order to form a long filament, the phase fluctuation of the laser beams should be as small as possible.

For convenience of indoor experiments, a converging lens is usually required to reduce the propagation distance before the on-set position of filaments. Thus the different local intensity peaks on the laser beam propagate with different direction. In order to investigate the effect of the crossing angle on the interaction, we model the propagation of two Gaussian pulses with different initial propagation direction for both cases of in-phase and out-of-phase. The envelope of the input pulse can be written as

$$E(x, y, z, t)|_{z=0} = E_0 e^{-[(x-\Delta_0/2)^2+y^2]/r_0^2 - t^2/\tau_0^2}$$

$$\times \exp\left(i\left(x - \frac{\Delta_0}{2}\right)\tan\theta\right)\exp(i\varphi)$$

$$+ E_0 e^{-[(x+\Delta_0/2)^2+y^2]/r_0^2 - t^2/\tau_0^2}$$

$$\times \exp\left(-i\left(x + \frac{\Delta_0}{2}\right)\tan\theta\right) \quad (5)$$

Fig. 8 The energy fluence distribution (J/cm^2) of two interacting Gaussian pulses with an initial separation distance $\Delta_0 = 0.8$ mm, individual incident angle θ, and relative phase shift φ; **a** $\theta = 0.01°$ and $\varphi = 0$, **b** $\theta = 0.01°$ and $\varphi = \pi$, **c** $\theta = 0.1°$ and $\varphi = 0$, **d** $\theta = 0.1°$ and $\varphi = \pi$. All the figures are plotted for the spatial slice at $y = 2.5$ mm
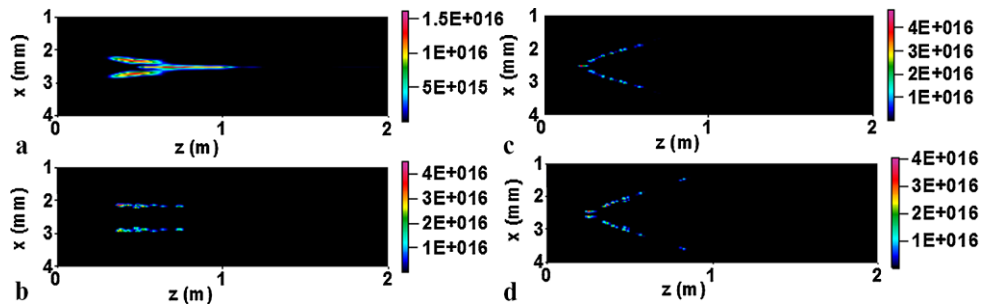
Fig. 9 The electron densities (/cm^3) for two interacting Gaussian pulses with an initial separation distance $\Delta_0 = 0.8$ mm, individual incident angle θ, and relative phase shift φ; **a** $\theta = 0.01°$ and $\varphi = 0$, **b** $\theta = 0.01°$ and $\varphi = \pi$, **c** $\theta = 0.1°$ and $\varphi = 0$, **d** $\theta = 0.1°$ and $\varphi = \pi$. All the figures are plotted for the spatial slice at $y = 2.5$ mm

where $\Delta_0 = 0.62$ mm is the initial separation distance, φ is the initial relative phase shift between the two pulses and θ represents the incident angle. Figure 8 shows the interaction of the laser beams with large incident angle ($\theta = 0.1°$) and small incident angle ($\theta = 0.01°$) for both in-phase and out-of-phase cases. For small incident angle $\theta = 0.01°$ (Fig. 8a), two collapsed pulses fuse into a long filament at the distance $z = 60$ cm, which is earlier than the case of the parallel pulses (Fig. 2c). For a large incident angle $\theta = 0.1°$ (Fig. 8c), the two in-phase pulses cross at $z = 25$ cm and then pass through each other. Figure 8b and d shows the interaction of two anti-phase pulses with large ($\theta = 0.1°$) and small ($\theta = 0.01°$) incident angles, respectively. Two anti-phase pulses with small incident angle propagate independently as shown in Fig. 8b. This is similar to the case of two parallel anti-phase pulses (Fig. 4a). Although the large incident angle makes the two anti-phase laser beams move close, they quickly repulse each other and then diverge. This situation is caused by quick change of the electron density in the interaction zone (Fig. 9d), where the balance between the Kerr self-focusing and de-focusing is broken. As a result, a long plasma channel can be formed by the two in-phase pulse with small cross angle (Fig. 9a).

4 Conclusion

In conclusion, the interaction of two intense fs Gaussian pulses in air was numerically investigated. For small separation distance and crossing angle, two in-phase pulses first self-focus into filaments and then fuse into one long filament. The length of the merged filament decreases with the increase of the phase shift between the pulses. For the out-of-phase case, two pulses repel each other and disperse quickly if the initial separation distance is small. When the separation distance is large, the filamentation of pulses developed independently. In addition, our simulation also indicates that for large crossing angle, two pulses meet, go through each other and then disperse quickly. Our simulation results can be helpful for understanding the influence of the initial intensity and phase modulation of laser pulses on the filamentation.

References

1. S.L. Chin, S.A. Hosseini, W. Liu, Q. Luo, F. Théberge, N. Aközbek, A. Becker, V.P. Kandidov, O.G. Kosareva, H. Schroeder, Can. J. Phys. **83**, 863 (2005)
2. T.T. Xi, J. Zhang, X. Lu, Z.Q. Hao, Q.L. Dong, H.C. Wu, Chin. Phys. **15**, 2025 (2006)
3. Z.Q. Hao, J. Zhang, Z. Zhang, T.T. Xi, Z.Y. Zheng, X.H. Yuan, Z.H. Wang, ACTA Phys. Sin. **54**, 3173 (2005)
4. R. Rairoux, H. Shillinger, S. Niedermeier, M. Rodriquez, F. Ronneberger, R. Sauerbrey, B. Stein, D. Waite, C. Wedekind, H. Wille, L. Wöste, C. Ziener, Appl. Phys. B **71**, 573 (2000)
5. J. Kasparian, M. Rodriguez, G. Méjean, J. Yu, E. Salmon, H. Wille, R. Bourayou, S. Frey, Y.B. André, A. Mysyrowicz, R. Sauerbrey, J.-P. Wolf, L. Wöste, Science **301**, 61 (2003)
6. M. Mlejnek, M. Kolesik, J.V. Moloney, E.M. Wright, Phys. Rev. Lett. **83**, 2938 (1999)
7. L. Bergé, S. Skupin, F. Lederer, G. Méjean, J. Yu, J. Kasparian, E. Salmon, J.-P. Wolf, M. Rodriguez, L. Wöste, R. Bourayou, R. Sauerbery, Phys. Rev. Lett. **92**, 225002 (2004)
8. V.I. Bespalov, V.I. Talanov, JETP Lett. **3**, 307 (1966)
9. T.T. Xi, X. Lu, J. Zhang, Phys. Rev. Lett. **96**, 025003 (2006)
10. S.L. Chin, S. Petit, W. Liu, A. Iwasaki, M.-C. Nadeau, V.P. Kandidov, O.G. Kosareva, K.Yu. Andrianov, Opt. Commun. **210**, 329 (2002)
11. S.A. Hosseini, Q. Luo, B. Ferland, W. Liu, S.L. Chin, O.G. Kosareva, N.A. Panov, N. Aközbek, V.P. Kandidov, Phys. Rev. A **70**, 033802 (2004)
12. S. Tzortzakis, L. Bergé, A. Couairon, M. Franco, B. Prade, A. Mysyowicz, Phys. Rev. Lett. **86**, 5450 (2001)
13. S. Skupi, L. Bergé, U. Peschel, F. Lederer, G. Méjean, J. Yu, J. Kasparian, E. Salmon, J.-P. Wolf, M. Rodriquez, L. Wöste, R. Bourayou, R. Sauerbrey, Phys. Rev. E **70**, 046602 (2004)
14. O.G. Kosareva, N.A. Panov, N. Akozbek, V.P. Kandidov, Q. Luo, S.A. Hosseini, W. Liu, J.-F. Gravel, G. Roy, S.L. Chin, Appl. Phys. B **82**, 111 (2006)
15. A. Dubietis, G. Tamošauskas, G. Fibich, B. Ilan, Opt. Lett. **29**, 1126 (2004)
16. G. Fibich, S. Eisenmann, B. Ilan, A. Zigler, Opt. Lett. **29**, 1172 (2004)
17. L. Bergé, M.R. Schmidt, J. Juul Rasmussen, P.L. Christiansen, K.Ø. Rasmussen, J. Opt. Soc. Am. B **14**, 2550 (1997)
18. A.A. Ishaaya, T.D. Grow, S. Ghosh, L.T. Vuong, A.L. Gaeta, Phys. Rev. Lett. **75**, 023813 (2007)